Improved magnetic anomalies of the Antarctic lithosphere from satellite and near-surface data

Hyung Rae Kim, Ralph R. B. von Frese, Patrick T. Taylor, Alexander V. Golynsky, Luis R. Gaya-Piqué, Fausto Ferraccioli

Geophys. J. Int. (2007) **171,** 119–126 doi: 10.1111/j.1365-246X.2007.03516.x

Improved magnetic anomalies of the Antarctic lithosphere from satellite and near-surface data

Hyung Rae Kim[1,2], Ralph R. B. von Frese[3], Patrick T. Taylor[2], Alexander V. Golynsky[4], Luis R. Gaya-Piqué[5] and Fausto Ferraccioli[6]

[1]*Goddard Earth Sciences and Technology Center, UMBC, Baltimore,* MD 21250*, USA. E-mail: kimhr@core2.gsfc.nasa.gov*
[2]*Code* 698*, Planetary Geodynamics Lab., NASA/GSFC, Greenbelt,* MD 20771*, USA*
[3]*School of Earth Sciences, The Ohio State University, Columbus,* OH 43210*, USA*
[4]*VNIIOkeangeologia,* 1*, Angliysky Ave., St. Petersburg,* 190121*, Russia*
[5]*Équipe de Géomagnétisme, IPGP, CNRS,* 2 *place Jussieu,* 75005 *Paris, France*
[6]*British Antarctic Survey, High Cross, Madingley Road, CB30ET Cambridge, UK*

Accepted 2007 June 5. Received 2007 June 5; in original form 2006 October 2

SUMMARY

The Antarctic magnetic anomaly map compiled marine and airborne surveys collected south of 60°S through 1999 and used Magsat data to help fill in the regional gaps between the surveys. Ørsted and CHAMP satellite magnetic observations with greatly improved measurement accuracies and temporal and spatial coverage of the Antarctic, have now supplanted the Magsat data. We combined the new satellite observations with the near-surface survey data for an improved magnetic anomaly map of the Antarctic lithosphere. Specifically, we separated the crustal from the core and external field components in the satellite data using crustal thickness variations estimated from the terrain and the satellite-derived free-air gravity observations. Regional gaps in the near-surface surveys were then filled with predictions from crustal magnetization models that jointly satisfied the near-surface and satellite crustal anomalies. Comparisons in some of the regional gaps that also considered newly acquired aeromagnetic data demonstrated the enhanced anomaly estimation capabilities of the predictions over those from conventional minimum curvature and spherical harmonic geomagnetic field models. We also noted that the growing number of regional and world magnetic survey compilations involve coverage gaps where these procedures can contribute effective near-surface crustal anomaly estimates.

Key words: ADMAP, Antarctic magnetic anomalies, near-surface surveys, satellite surveys.

INTRODUCTION

Magnetic data provide critical insights on the geology of Antarctica, where the harsh environment and extensive ice cover greatly limit conventional field mapping. The Working Group of the Antarctic Digital Magnetic Anomaly Project (ADMAP) compiled a magnetic anomaly map for the region south of 60°S from roughly 1.5 million line-kilometres of airborne and marine survey data and about 5.6 million line-kilometres of Magsat satellite data (Golynsky *et al.* 2001, 2006).

Fig. 1 gives the ADMAP compilation from the 5-km magnetic anomaly grid that is publicly available on-line (http://earthsciences.osu.edu/admap). The prominent regional anomalies indicate the gaps in the near-surface survey coverage. They were filled in by predictions from crustal magnetization models that jointly satisfied the 400-km low-pass filtered near-surface survey data and the 400-km altitude Magsat crustal anomaly estimates (Golynsky *et al.* 2001). Recently, however, new higher accuracy and more numerous satellite magnetic observations at roughly 700 and 400 km altitudes from the Ørsted and CHAMP missions, respectively, have superseded Magsat observations for estimating Antarctic crustal anomalies (Kim *et al.* 2004a).

The Magsat data yielded problematic Antarctic crustal anomaly estimates because the mission operated only over austral summer and fall, when the large external fields most strongly corrupted and distorted the relatively weak crustal anomalies. The short 6-month Magsat mission collected a limited amount of data, in contrast to the currently operating Ørsted and CHAMP missions that have obtained several years of data including magnetically quiet austral winter observations.

In addition, the magnetometers aboard the Ørsted and CHAMP satellites have accuracies better than 0.5 nT, which is an order of magnitude greater than Magsat's (Neubert *et al.* 2001; Reigber *et al.* 2002). Thus, Ørsted and CHAMP observations can improve the accuracy of the crustal anomaly estimates in the coverage gaps of the near-surface Antarctic surveys. Theoretical analysis of the measurement errors, for example, indicates that the respective Ørsted and CHAMP-based near-surface anomaly estimates can be

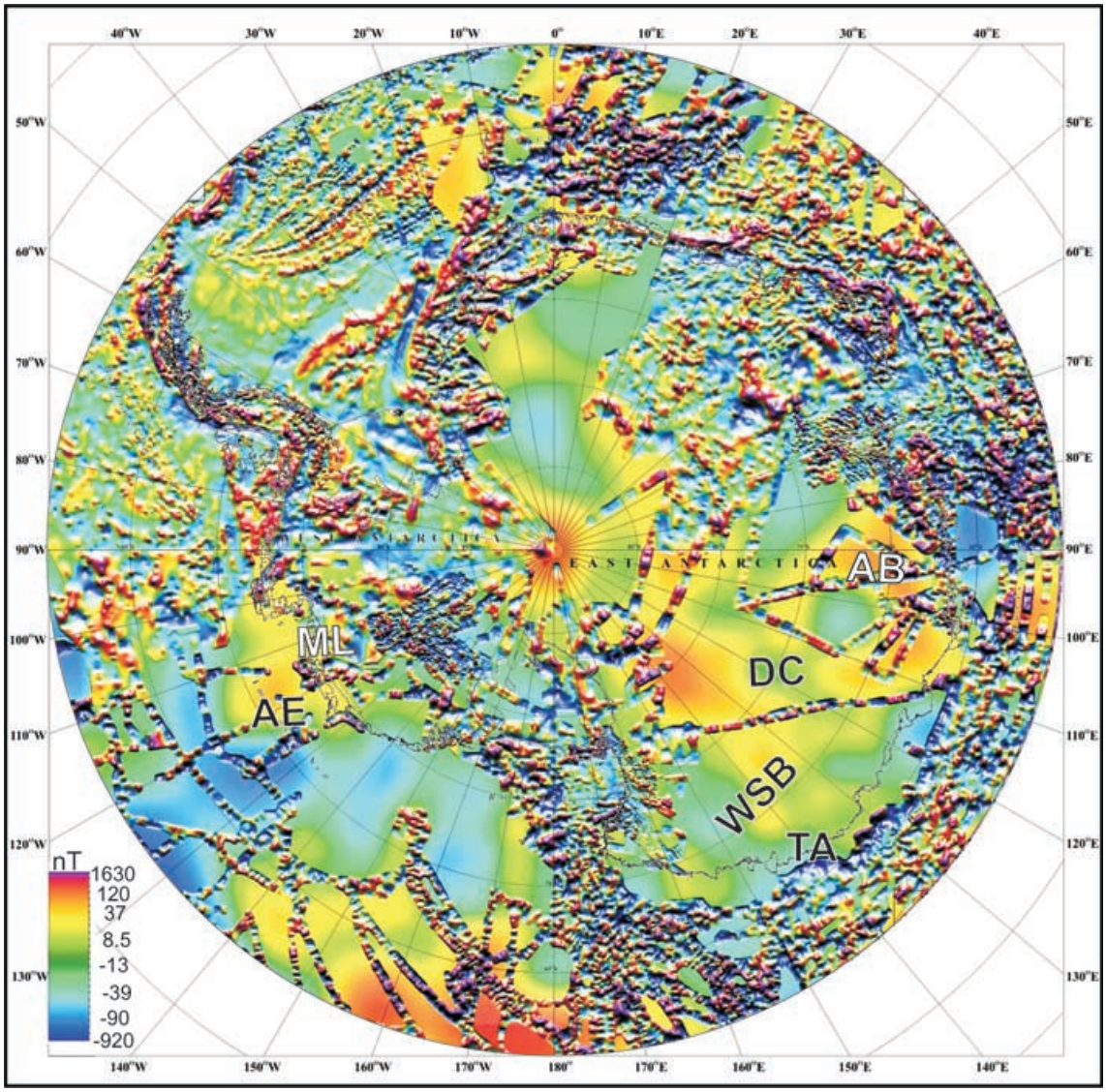

Figure 1. Total field magnetic anomalies of the Antarctic gridded at the interval and effective altitude of 5 km (Golynsky *et al.* 2001). The high-frequency anomalies illustrate the coverage of the near-surface surveys up through 1999. The low-frequency components delineate the regional gaps that were filled in with anomaly estimates from the joint inversion of Magsat and near-surface data. The feature annotations include AB (Aurora Basin), AE (Amundsen Sea Embayment), DC (Dome C), ML (Marie Byrd Land), TA (Terre Adelie) and WSB (Wilkes Subglacial Basin).

roughly 12 and 76% more accurate than the corresponding Magsat-based predictions (Kim *et al.* 2004a).

We have updated the ADMAP compilation with improved gap predictions that jointly satisfy crustal anomaly estimates of the near-surface and Ørsted and CHAMP satellite magnetic surveys. We describe the procedures for extracting crustal anomalies from satellite magnetic data and computing least-squares estimates of crustal anomalies from multi-altitude magnetic surveys. These anomaly estimates are not unique and thus to test their veracity we compare them with newly acquired airborne survey data for some of the gaps.

EXTRACTING ANTARCTIC CRUSTAL MAGNETIC ANOMALIES FROM SATELLITE OBSERVATIONS

The near-surface components of the ADMAP compilation tend to reflect local to regional scale geological features that satellite-derived magnetic observations can only partly detect. In addition, for the polar regions, the behaviour of the strong and complex external magnetic field components (e.g. field-aligned currents and the polar electrojet) is inferred from global observatory data that poorly covers Antarctica (Sabaka *et al.* 2004; Maus *et al.* 2006). Hence global spherical harmonic models of crustal anomalies derived from magnetically quiet satellite observations only marginally account for the behaviour of auroral fields (von Frese & Kim 2003).

For effective near-surface estimates, the Antarctic crustal anomaly details need to be assessed as accurately as possible. Thus, more local crustal constraints must be invoked than are normally considered in producing standard global spherical harmonic geomagnetic field models from satellite data. For example, effective separation of local crustal and core components must account for the spectral overlap of the core field with the magnetic effects of crustal thickness variations (Meyer *et al.* 1983; von Frese *et al.* 1999a). Furthermore, the effects of crustal sources include the

positively correlated anomaly features on neighbouring orbits separated by small distances relative to altitude, whereas non-crustal effects include the null-to-negatively correlated data components between these passes (Alsdorf *et al.* 1994).

To reduce the satellite magnetic observations for core field effects, we used the CM4 model (Sabaka *et al.* 2004). The power spectrum in the CM4 model breaks mainly into two slopes that represent mostly core and the crustal field effects. However, the two slopes of the spectrum overlap significantly between spherical harmonic degrees 14–17. Thus, we removed the first-order core component up to degree 14 along each data track in local magnetic time bins (e.g. dawn and dusk orbits). The residuals, however, still contain higher order Antarctic core field effects mixed in with non-crustal signals and crustal anomalies from density contrasts due to intracrustal sources and thickness variations of the crust (von Frese *et al.* 1999a; Kim *et al.* 2004b).

To estimate the regional crustal thickness effects in the Ørsted and CHAMP track residuals, we modelled the magnetic effects of Antarctic crustal thickness variations from von Frese *et al.* (1999b). These crustal thickness estimates were obtained by the Moho inversion of isostatically adjusted complete Bouguer anomalies where the computed gravity effects of the ice, water and rock components of the terrain were subtracted from free-air gravity anomalies that were strongly correlated with the terrain gravity effects. The analysis presumed that the terrain-correlated free-air anomalies reflected isostatically disturbed crustal terrain and yielded Moho estimates that were well within several percent of the available seismic Moho estimates (von Frese *et al.* 1999b).

We used a constant susceptibility contrast to obtain preliminary magnetic effects of the Antarctic crustal thickness variations. However, to estimate the actual crustal thickness magnetic effects, we used correlation filters (von Frese *et al.* 1997) to extract all wavenumber components in the satellite observations that were positively correlated with the preliminary crustal thickness magnetic effects. These estimates were removed from the first-order CHAMP and Ørsted residuals and converted into maps of Antarctic crustal thickness magnetic effects at 400 and 700 km, respectively.

Removal of the estimated crustal thickness magnetic effects yielded second-order residuals in the satellite observations with low-order regional trends that we ascribed to residual core field and long-wavelength external field effects. To suppress these effects, we fit and removed first-order linear trends from each of the track residuals. The resulting third-order residuals contain essentially the effects of dynamic external fields and temporally and spatially static magnetization variations within the crust.

The static intracrustal anomalies correlate positively between orbital data tracks separated by small distances relative to altitude, whereas null or negatively correlated features on these tracks must be related to the dynamic effects of external fields and other non-crustal noise. To extract the positively correlated data components, we applied spectral correlation filters using the correlation spectrum between the two data tracks defined from the phase differences in the spectral components (Alsdorf *et al.* 1994; von Frese *et al.* 1997). Enhancing the correlation between two neighbouring data tracks improves the ratio of lithospheric signal (S)-to-non-lithospheric noise (N) as $\mathrm{N/S} \approx \sqrt{(|\mathrm{CC}|^{-1} - 1)}$, where CC is correlation coefficient between the data (Foster & Guinzy 1967; Kim 1995). We then used least-squares collocation (Goyal *et al.* 1990) to construct maps at common altitude and spherical coordinates from the correlated observations.

These enhancements yielded Ørsted and CHAMP anomaly maps dominated by intracrustal magnetic effects that when added to the relevant crustal thickness magnetic effects produce the comprehensive crustal anomaly maps in Figs 2(A) and (B), respectively. These anomaly maps provide critical boundary conditions in using the near-surface magnetic data for estimating effective crustal anomaly values in the regional coverage gaps of the surveys.

NEAR-SURFACE CRUSTAL ANOMALY ESTIMATES IN THE COVERAGE GAPS

In this study, we processed the Ørsted and CHAMP data collected over the Antarctic during 2002 and 2003 for their crustal anomaly components. The effects of sources producing near-surface anomalies with wavelengths shorter than about 400 km altitude are not detectable in the lower altitude CHAMP satellite observations (e.g. Ravat *et al.* 2002; Kim *et al.* 2004a). Thus, to supplement the satellite constraints on the gap predictions, we used the near-surface survey anomalies low-pass filtered for wavelengths roughly 400 km and larger shown in Fig. 2(C).

We developed the gap estimates from the predictions of a crustal magnetization model of crustal prisms $1.5^\circ \times 1.5^\circ$ wide and 30-km thick, with magnetizations obtained from the inversion of the crustal anomalies in Figs 2(A)–(C). Following Ravat *et al.* (2002), we obtained minimum mean-squared error estimates of the prism magnetizations ($\mathbf{X}$) from

$$\mathbf{X} = [\mathbf{A}^{\mathrm{T}}\mathbf{w}\mathbf{A} + \lambda\mathbf{I}]^{1}\mathbf{A}^{\mathrm{T}}\mathbf{w}\mathbf{B},$$

where the design matrix $\mathbf{A} = [\mathbf{A_{AD}}\ \mathbf{A_C}\ \mathbf{A_Ø}]^{\mathbf{T}}$ includes the near-surface ($\mathbf{A_{AD}}$), CHAMP ($\mathbf{A_C}$) and Ørsted ($\mathbf{A_Ø}$) submatrices that reflect the geometric relationships between the crustal prism and observation coordinates as modelled by Gauss–Legendre quadrature integration (von Frese *et al.* 1981). Similarly, the column vector of observations $\mathbf{B} = [\mathbf{B_{AD}}\ \mathbf{B_C}\ \mathbf{B_Ø}]^{\mathbf{T}}$ is made up of subvectors that represent the magnetic anomaly observations from the near-surface ($\mathbf{B_{AD}}$), CHAMP ($\mathbf{B_C}$) and Ørsted ($\mathbf{B_Ø}$) surveys. The diagonal weighting matrix $\mathbf{w} = [\mathbf{w_{AD}}\ \mathbf{w_C}\ \mathbf{w_Ø}]^{\mathbf{T}}$ includes subvectors to process the three elements of the design matrix at essentially full working precision.

We used the identity matrix $\mathbf{I}$ multiplied by the scalar error variance or damping factor λ to help manage the stability of the solution. Specifically, we developed performance diagrams comparing the correlation coefficients (CC) and root mean squared (rms) differences between predicted and observed anomalies for different λ-values. We took as essentially 'optimal' those λ-values with solutions of maximum CC and minimum rms difference between predictions and observations. Table 1 gives the performance statistics used for making the predictions in each of the gaps.

In making the gap predictions, we developed an initial crustal magnetization model with this approach that comprehensively satisfied the available multi-altitude crustal anomalies in Figs 2(A)–(C). At each of the six gaps, however, we tuned the error variance slightly to optimize the fit of the near-surface predictions with the related observations around the boundary of the gap. Using the tuned error variance, we estimated the crustal anomalies at the desired near-surface coordinates within the gaps (Fig. 2D).

Fig. 2(D) shows the gap predictions from the tuned inversions of the Ørsted and CHAMP satellite and near-surface survey data. The regional gap predictions incorporating satellite altitude magnetic observations are far superior to conventional interpolations of near-surface observations (Kim *et al.* 2004a). However, our gap predictions are not unique due to the data and modelling errors and the inherent source ambiguity of magnetic anomalies. Thus, to test the significance of these predictions, we compare them in the next

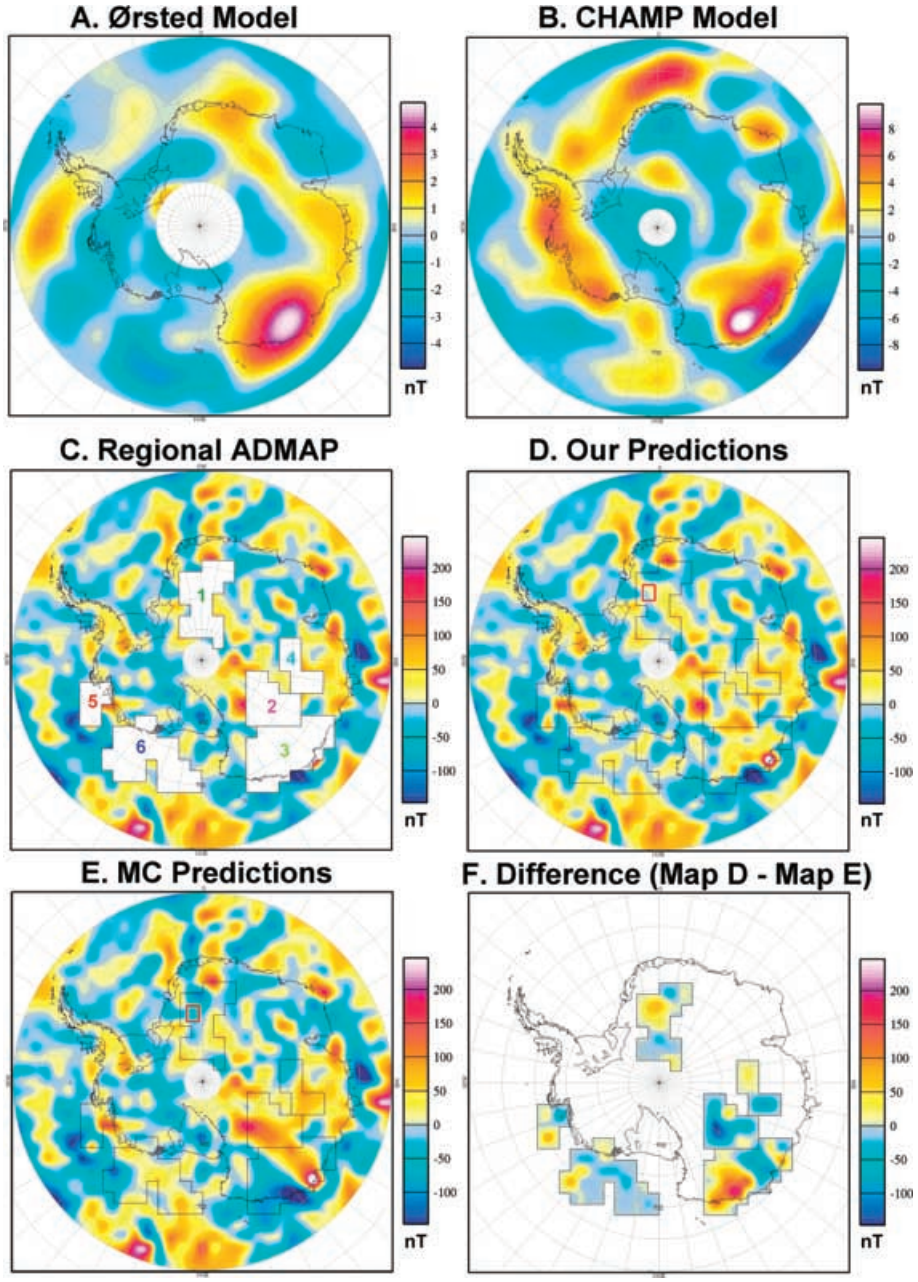

Figure 2. (A) Ørsted scalar magnetic anomaly map at 700 km. (B) CHAMP scalar magnetic anomaly map at 400 km altitude. (C) Long wavelength (>400 km) ADMAP data with numerically marked coverage gaps. (D) ADMAP magnetic anomaly map with the coverage gaps filled in by the joint inversion of the data from Maps A, B and C. (E) ADMAP magnetic anomaly map with coverage gaps filled in by minimum curvature interpolation. (F) Differences in the gap anomaly estimates obtained by subtracting Map E from Map D.

Table 1. Error variances (λ) used for each set of our gap predictions, and the corresponding maximum correlation coefficient (CC), and minimum rms difference (rms in nT) between the predictions and observations along the gap's periphery.

Gaps	#1	#2	#3	#4	#5	#6
$\log_{10}(\lambda)$	9.75	9.5	10	9.5	9.25	10
CC	0.52	0.79	0.66	0.73	0.78	0.73
rms (nT)	43.3	38.6	59.2	30.8	45.7	27.2

section with available geological constraints and newly acquired aeromagnetic data.

DISCUSSION

The large coverage gaps in Fig. 2(C) include the region east of the Shackleton Range (#1), Wilkes Land (#2 and #3), and portions of the Aurora Subglacial Basin (#4) in East Antarctica, as well as on- and off-shore regions of Marie Byrd Land (#5) and the Amundsen Sea Embayment (#6) in West Antarctica. We do not consider the central void south of 87°S in our analysis because the orbital inclinations of the missions were too low to cover it.

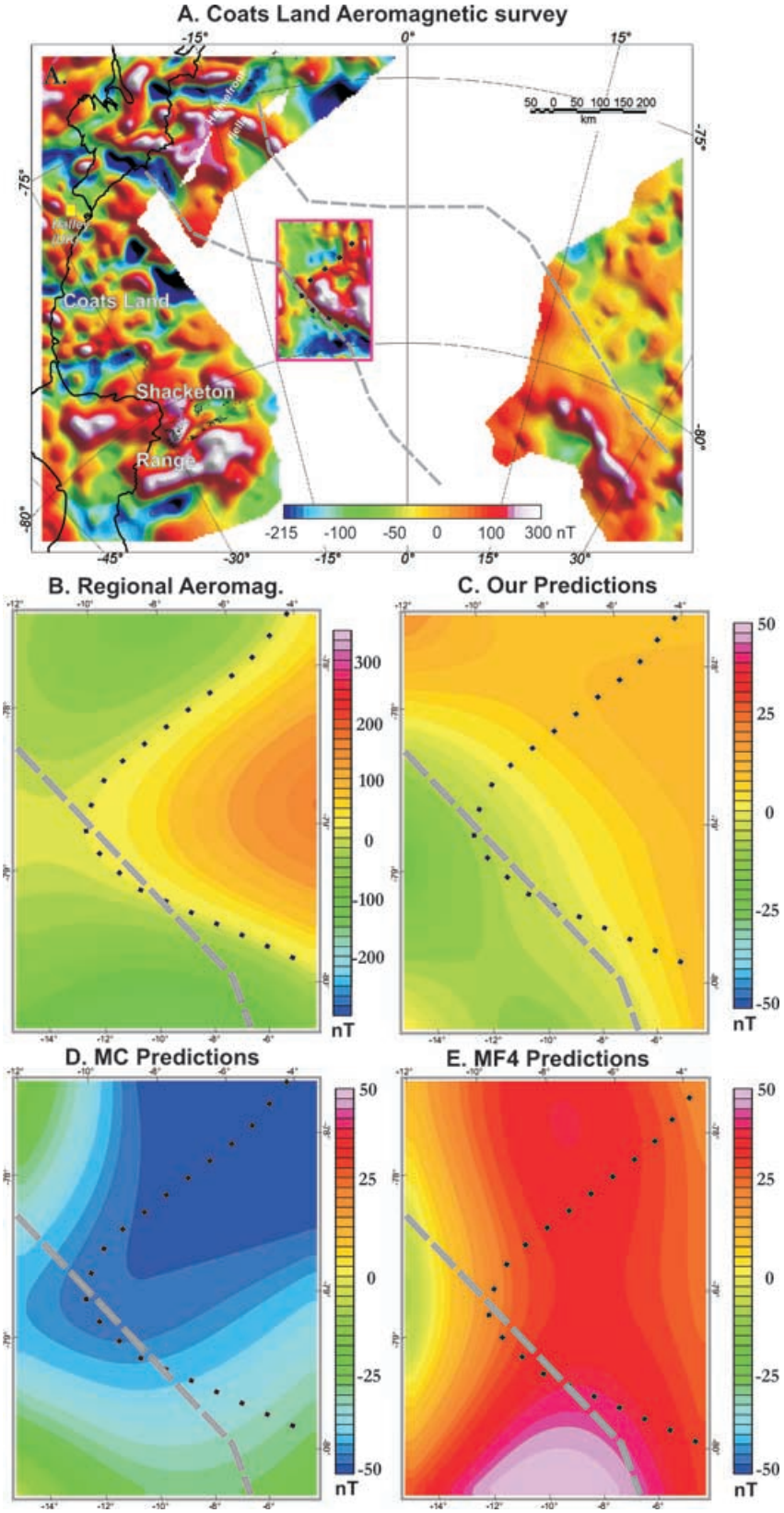

Figure 3. Comparisons of magnetic anomaly predictions within a recently surveyed portion of the regional gap #1 located east of Coats Land and the Shackleton Range in East Antarctica. (A) Recently, surveyed aeromagnetic anomalies within the red-bordered area (Shepherd *et al.* 2006) are part of a NW–SE trending, positive regional anomaly complex predicted in Fig. 2(D) within the area between the dashed grey lines. (B) The regional anomaly components of the new aeromagnetic data low-pass filtered for 200-km and longer wavelengths. The black dotted line delineates the regional magnetic high from Map A. (C) Our anomaly estimates over the newly surveyed area. (D) Anomaly estimates from minimum curvature. (E) Anomaly estimates from the spherical harmonic geomagnetic field model MF4 (Maus *et al.* 2006).

Table 2. Correlation coefficients between the regional aeromagnetic anomalies (Fig. 3B), our predictions (Fig. 3C), the minimum curvature estimates (Fig. 3D) and the predictions from the spherical harmonic geomagnetic field model MF4 (Fig. 3E).

Maps	Fig. 3B	Fig. 3C	Fig. 3D	Fig. 3E
Fig. 3B	1	0.45	−0.50	−0.18
Fig. 3C		1	−0.40	0.22
Fig. 3D			1	0.05
Fig. 3E				1

Table 3. Correlation coefficients within (and outside) the Antarctic gaps between our predictions (Fig. 2D), the minimum curvature estimates (Fig. 2E) and the 5-km altitude estimates from the spherical harmonic geomagnetic field models MF4 (Maus *et al.* 2006) and CM4 (Sabaka *et al.* 2004). The range of spherical harmonic degrees for which these global field models were evaluated is given in parentheses.

Predictions	Fig. 2D	MF4	CM4	Fig. 2E
Fig. 2D	1	0.21 (0.31)	0.43 (0.22)	0.03 (1.00)
MF4 (16–90)		1	0.46 (0.50)	−0.10 (0.31)
CM4 (16–65)			1	0.08 (0.22)
Fig. 2E				1

Testing the geological veracity of our gap predictions in Fig. 2(D) is difficult because of the paucity of outcrop and independent geophysical constraints. However, alternate predictions from different approaches can provide useful added perspective and contrast on the interpretational options that are possible for the data. Thus, for the discussion below we include the gap predictions by minimum curvature (Smith & Wessel 1990) in Fig. 2(E) and also consider the differences in Fig. 2(F) between the two sets of predictions.

For gap #1, Fig. 3 compares newly collected aeromagnetic survey data against the predictions. The red-bordered area within the gap of Fig. 3(A) shows the new data mapped by the British Antarctic Survey (Shepherd *et al.* 2006). The positive regional magnetic anomaly is comparable to the magnetic effects observed to the southwest for the high-grade metamorphic rocks of the Shackleton Range (Hunter *et al.* 1996). However, our gap predictions in Fig. 2(D) suggest that the positive regional anomaly is part of a positive anomaly complex that is roughly located between the dashed grey lines in Fig. 3(A). Thus, the newly mapped positive anomaly may represent a different crustal domain where generally NW–SE anomaly trends prevail rather than the mostly E–W trends of the Shacketon Range.

Fig. 3(B) shows the more regional anomaly properties of the newly collected aeromagnetic data that were obtained by low-pass filtering for wavelengths of about 200 km and larger. The heavy dotted line broadly outlines the prominent positive regional anomaly in Fig. 3(A). Table 2 summarizes the correlations between the regional anomalies (Fig. 3B) and our predictions (Fig. 3C), the minimum curvature estimates (Fig. 3D) and the CHAMP global spherical harmonic model MF4 (Maus *et al.* 2006) predictions (Fig. 3E). Our estimates clearly have the greatest sensitivity for the regional components of the newly mapped aeromagnetic data in the gap. The minimum curvature (MC) predictions, on the other hand, reflect the simple, but effectively meaningless interpolation of the near-surface observations across the gap. The MF4 model is likewise unconstrained by the near-surface data and thus also yields quite limited gap predictions.

Gaps #2 and #3 in the Wilkes Land area of East Antarctica give the greatest differences between the minimum curvature and satellite-based predictions (Fig. 2F). The BEDMAP compilation of subice topography (Lythe *et al.* 2001) shows that the main subice feature of the region is the Wilkes Subglacial Basin (WSB in Fig. 1). The crustal properties of the basin are poorly known and may involve an extended terrane with thin sedimentary infill (Ferraccioli *et al.* 2001), or a flexural depression with no sediments (ten Brink *et al.* 1997). Magsat and ground-based magnetic data suggest that it may be underlain by Neoproterozoic(?) basement of the Ross Orogen which is weakly magnetic in contrast to highly magnetic Precambrian cratonic basement to the east (Ferraccioli *et al.* 2001).

The large differences in the two sets of gap predictions infer sharply contrasting crustal interpretations for the WSB. For example, the minimum curvature predictions in Fig. 2(E) appear to delineate a prominent lineament separating a regional magnetic low over the basin from the magnetic high to the east. However, our satellite-based predictions in Fig. 2(D) suggest a more subdued boundary along the basin's eastern margin with magnetic highs over parts of the basin, as well as the Dome C plateau (Bentley *et al.* 1983). Recently, acquired aeromagnetic data over the southern WSB have imaged comparable magnetic highs (Studinger *et al.* 2004) that may reflect Precambrian basement. In addition, the regional magnetic high that we estimate over the Terre Adelie (TA) coast may mark the extent of the Precambrian Mawson block (Finn *et al.* 2006).

For gap #4 in the East Antarctic and gaps #5 and #6 of the West Antarctic, substantial differences in the two sets of predictions are evident that range over about 150 nT (Fig. 2F). Unfortunately, the cover of ice and seawater and the lack of independent geophysical observations make it very difficult to develop meaningful assessments of the geological implications of the predictions. However, in contrast to other approaches, the gap predictions in Fig. 2(D) invoke all available crustal magnetic anomaly constraints.

For example, Table 3 summarizes the correlations of our gap predictions (Fig. 2D) with the minimum curvature estimates (Fig. 2E), as well as the 5-km altitude predictions from the widely used spherical harmonic geomagnetic field models CM4 (Sabaka *et al.* 2004) and MF4 (Maus *et al.* 2006). The coefficients without parentheses in Table 3 refer to the correlations within the gaps, whereas the values in parentheses refer to the correlations outside the gaps.

Table 3 reveals an almost total lack of correlation between the minimum curvature and our gap predictions that clearly demonstrates the potential effectiveness of the satellite data for constraining near-surface crustal magnetic anomalies. The CM4 and MF4 models also are poorly constrained by near-surface magnetic observations over the Antarctic. Thus, their estimates correlate only marginally with the near-surface crustal anomalies outside the gaps (Fig. 2C), although within the gaps, the CM4 estimates correlate somewhat better with our predictions than the MF4 estimates. However, essentially lacking near-surface crustal anomaly data over the Antarctic, the global spherical harmonic model estimates can provide only a very limited description of the near-surface crustal anomaly field.

In Fig. 4, we offer our best current estimate of the near-surface Antarctic crustal magnetic anomaly field. For this map, we added back to Fig. 2(D) the wavelength components shorter than about 400 km that had been high-cut filtered from the near-surface observations to produce Fig. 2(C). Improvements in this map will result from improvements in the near-surface and satellite survey coverage. New surveying since the production of the initial map in Fig. 1, for example, has essentially doubled the amount of near-surface magnetic anomaly observations for the Antarctic (von Frese *et al.* 2007). Also, as the satellite missions move to completion, the orbital altitudes will be reduced to reveal more crustal anomaly

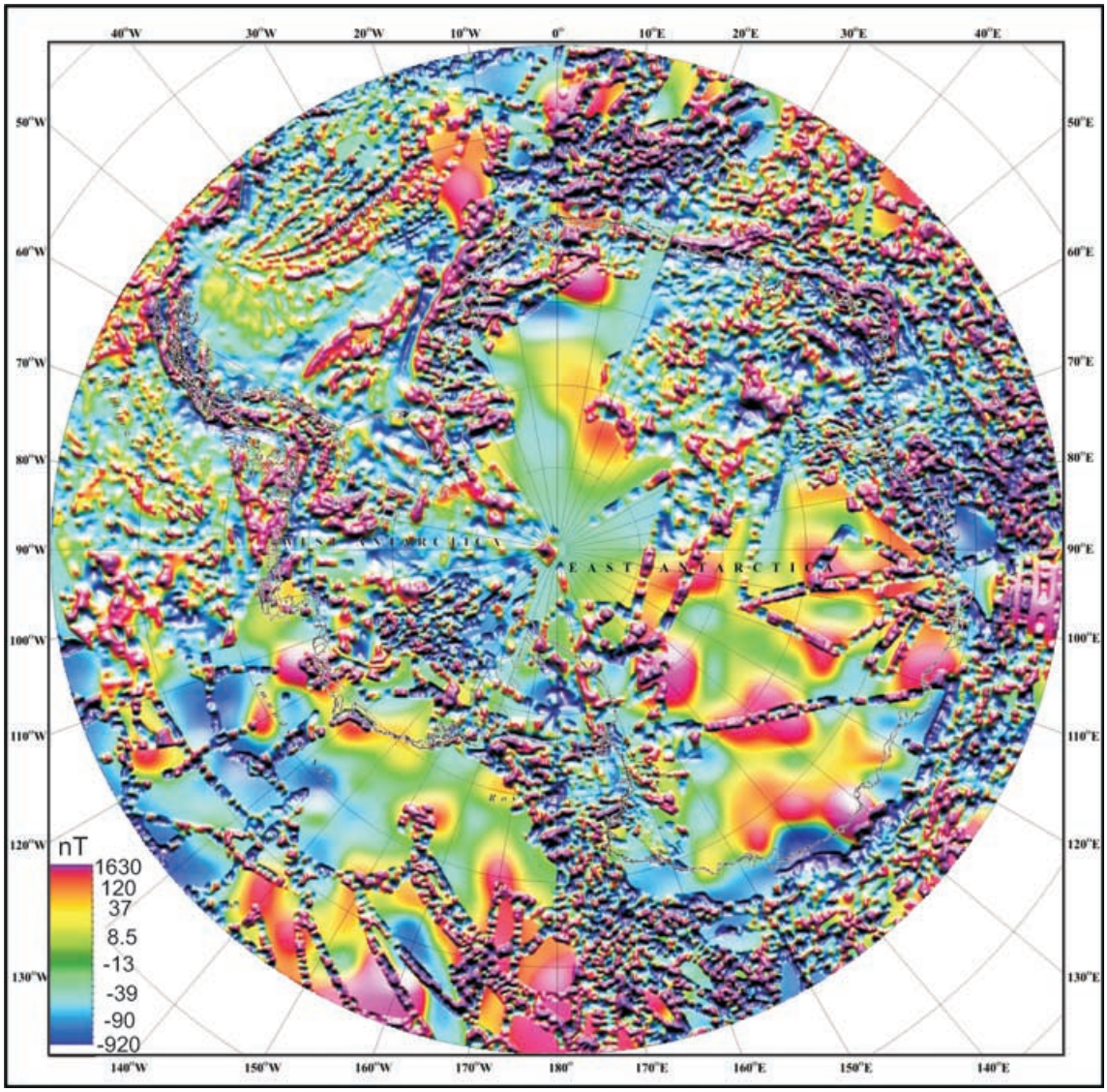

Figure 4. The updated magnetic anomaly map of the Antarctic with the coverage gaps filled in by the joint inversion of near-surface, CHAMP and Ørsted satellite observations.

details. Thus, momentum is building for a new generation Antarctic magnetic anomaly map that incorporates these developments.

CONCLUSIONS

The greatly improved accuracy of Ørsted and CHAMP data over the Magsat data warrants their use for estimating anomalies in regional coverage gaps of the near-surface magnetic surveys in the ADMAP compilation. Accordingly, we adapted CHAMP data at 400 km and Ørsted data at 700 km to fill in the near-surface data gaps (Fig. 2D) and compiled an improved magnetic anomaly map for Antarctica (Fig. 4). Our estimates for the gap to the east of the Shackleton Range are generally consistent with the long-wavelength components of an aeromagnetic survey of part of this gap. The predictions over Wilkes Land are also consistent with recently acquired aeromagnetic data. Thus, our predictions may help to delineate contrasting lithospheric blocks of the East Antarctic Craton.

Regional compilations of near-surface magnetic survey data are becoming increasingly available like those for North America (Bankey *et al.* 2002), Africa (Barritt *et al.* 1993), Europe (Wonik *et al.* 2001), Australia (Milligan & Tarlowski 1999) and other places. Indeed, current major initiatives include the World Magnetic Anomaly Map (Ravat *et al.* 2003) and the ongoing Antarctic magnetic map compilation (von Frese *et al.* 2007). These compilations involve regional coverage gaps that may be filled in with relevant crustal anomaly estimates from Ørsted and CHAMP magnetic observations using the procedures developed in this study.

Our gap predictions are limited by the errors in reducing magnetic observations for their lithospheric components and the restricted anomaly detail that satellite observations can resolve. However, accurate satellite crustal magnetic observations in combination with near-surface data can provide better low-altitude anomaly estimates in unsurveyed areas than is possible to obtain from the near-surface data alone.

ACKNOWLEDGMENTS

This study was produced under the auspices of the ADMAP, which operates under supporting resolutions of the International

Association of Geomagnetism and Aeronomy (IAGA) and as an Expert Group of the Scientific Committee on Antarctic Research (SCAR). Aspects of this study were supported by NASA grant NNG04GQ44G to HRK and NSF grant OPP 0338005 to RvF. We thank G. Eagles and an anonymous reviewer for their constructive comments on this paper.

REFERENCES

Alsdorf, D.E., von Frese, R.R.B., Arkani-Hamed, J. & Noltimier, H.C., 1994. Separation of lithospheric, external, and core components of the south polar geomagnetic field at satellite altitudes, *J. Geophys. Res.*, **99,** 4655–4667.

Bankey, V., *et al*., 2002. Digital data grids for the magnetic anomaly map of N. America, *USGS Open File Report*, 02-414.

Barritt, S.A., Fairhead, J.D. & Misener, D.J., 1993. The African magnetic mapping project (AMMP), *ITC J.*, 122–131.

Bentley, C., Shabtaie, S., Lingle, C. & Blankenship, D., 1983. Analysis of geophysical data from Dome C and the Ross Ice Shelf, *Antar. J.U.S.*, **18,** 104–105.

Ferraccioli, F., *et al*., 2001. Rifted(?) crust at the East Antarctic Craton margin: gravity and magnetic interpretation along a traverse across the Wilkes Subglacial Basin region, *Earth Planet. Sci. Lett.*, **192,** 407–421.

Finn, C.A., Goodge, J.W., Damaske, D. & Fanning, C.M., 2006. Scouting cratons's edge in paleo-Pacific Gondwana, in *Antarctica: Contributions to Global Earth Sciences*, pp. 165–174, eds Futterer, D.K., Damaske, D., Gleinschmidt, G., Miller, H. & Tessensohn, F., Springer-Verlag.

Foster, M.R. & Guinzy, N.J., 1967. The coefficient of coherence: its estimation and use in geophysical prospecting, *Geophysics*, **32,** 602–616.

Golynsky, A. & ADMAP Working Group, 2001. ADMAP—magnetic anomaly map of the Antarctic, 1:10.000.000 scale map, *BAS Misc.* **10,** Cambridge, British Antarctic Survey.

Golynsky, A., & ADMAP Working Group, 2006. ADMAP—a digital magnetic anomaly map of the Antarctic, in *Antarctica: Contributions to Global Earth Sciences*, pp. 93–104, eds Futterer, D.K., Damaske, D., Gleinschmidt, G., Miller, H. & Tessensohn, F., Springer-Verlag.

Goyal, H.K., von Frese, R.R.B. & Hinze, W.J., 1990. Statistical prediction of satellite magnetic anomalies, *Geophys. J. Int.*, **102,** 101–111.

Hunter, R.J., Johnson, A.C. & Aleshkova, N.D., 1996. Aeromagnetic data from the southern Weddell Sea embayment and adjacent areas: synthesis and interpretation, in *Weddell Sea Tectonics and Gondwana Break-up (Geol. Soc. Sp. Pub. V. 108)*, pp. 143–154, eds B. Storey, E. King & R. Livermore, Geological Society London, London.

Kim, J.-H., 1995. Improved recovery of gravity anomalies from dense altimeter data, *PhD thesis*. The Ohio State University, Columbus, Ohio.

Kim, H.R., von Frese, R.R.B., Taylor, P.T., Kim, J.W. & Neubert, T., 2002. Ørsted verifies regional magnetic anomalies of the Antarctic lithosphere, *Geophys. Res. Lett.*, **29,** ORS 3-1–3-3

Kim, H.R., von Frese, R.R.B., Taylor, P.T., Golynsky, A.V. & Kim, J.W., 2004a. Application of satellite magnetic observations for estimating near-surface magnetic anomalies, *Earth, Planet. Space*, **56,** 955–966.

Kim, H.R., von Frese, R.R.B., Taylor, P.T., Kim, J.W. & Golynsky, A.V., 2004b. Near-surface magnetic predictions using CHAMP and Ørsted magnetometer data over Antarctica, *Abstract, 3rd CHAMP and GRACE Joint Scientific Meeting*, Potsdam, Germany.

Lythe, M., Vaughan, D. & BEDMAP Consortium, 2001. BEDMAP: a new ice thickness and subglacial topographic model of Antarctica, *J. Geophys. Res.*, **106,** 11 335–11 352.

Meyer, J., Hufen, J.-H., Siebert, M. & Hahn, A., 1983. Investigations of internal geomagnetic field by means of a global model of the Earth's crust, *J. Geophys.*, **52,** 71–84.

Maus, S., *et al*., 2006. Earth's lithospheric magnetic field determined to spherical harmonic degree 90 from CHAMP satellite measurements, *Geophys. J. Int.*, **164,** 319–330.

Milligan, P.R. & Tarlowski, C., 1999. *Magnetic Anomaly Map of Australia*, 3rd edn, scale 1: 5000000, Australian Geological Survey Organization, Canberra.

Neubert, T., *et al*., 2001. Ørsted satellite captures high-precision geomagnetic field data, *EOS (Am. Geophys. Union Trans.)*, **82,** 81–88.

Ravat, D.N., Whaler, K.A., Pilkington, M., Sabaka, T.J. & Purucker, M.E., 2002. Compatibility of high-altitude aeromagnetic and satellite-altitude magnetic anomalies over Canada, *Geophysics*, **67,** 546–554.

Ravat, D., *et al*., 2003. Toward the world digital magnetic anomaly map, *Eos Trans. AGU*, **84**(46), Fall meet. Suppl., Abstract GP21D-01.

Reigber, C., Lühr, H. & Schwintzer, P., 2002. Champ mission status, *Adv. Space Res.*, **30,** 129–134.

Sabaka, T.J., Olsen, N. & Purucker, M., 2004. Extending comprehensive models of the Earth's magnetic field with Ørsted and CHAMP data, *Geophys. J. Int.*, **159,** 521–547.

Shepherd, T., Bamber, J.L. & Ferraccioli, F., 2006. Subglacial geology in Coats Land, East Antarctica, revealed by airborne magnetics and radar sounding, *Earth. Planet. Sci. Lett.*, **244,** 323–335.

Smith, W.H. & Wessel, P., 1990. Gridding with continuous curvature splines in tension, *Geophysics*, **55,** 293–305.

Studinger, M., Bell, R., Buck, W., Karner, G. & Blankenship, D., 2004. Sub-ice geology inland of the Transantarctic Mountains in light of new aerogeophysical data, *Earth. Planet. Sci. Lett.*, **220,** 391–408.

ten Brink, U.S., *et al*., 1997. Uplift of the Transantarctic Mountains and the bedrock beneath the East Antarctic ice sheet. *J. Geophys. Res.*, **102,** 27 603–27 621.

von Frese, R.R.B., Hinze, W.J., Braile, L.W. & Luca, A.J., 1981. Spherical-earth gravity and magnetic anomaly modeling by Gauss-Legendre quadrature integration, *J. Geophys.*, **49,** 234–242.

von Frese, R.R.B., Jones, M.B., Kim, J.W. & Kim, J.-H., 1997. Analysis of anomaly correlations, *Geophysics*, **62,** 342–351.

von Frese, R.R.B., *et al*., 1999a, Satellite magnetic anomalies of the Antarctic crust, *Ann. di Geofis.*, **42,** 309–326.

von Frese, R.R.B., Tan, L., Kim, J.W. & Bentley, C.R., 1999b, Antarctic crustal modeling from the spectral correlation of free-air gravity anomalies with the terrain, *J. Geophys. Res.*, **104,** 25 275–25 296.

von Frese, R.R.B. & Kim, H.R., 2003. Satellite magnetic anomalies for lithospheric exploration, in *Proc. 4th Ørsted Int. Sci.Team Conf.*, pp. 115–118, eds P. Stauning *et al.*, Narayana.

von Frese, R.R.B. & the ADMAP Working Group, 2007. The next generation Antarctic digital magnetic anomaly map, in *Proc. ISAES07*, in-press.

Wonik, T., *et al*., 2001. Magnetic anomaly map for northern, western and eastern Europe, *Terra Nova*, **13,** 203–213.